TISSUE ENGINEERING: Part A
Volume 18, Numbers 13 and 14, 2012

DOI: 10.1089/ten.tea.2011.0076

Optimally Porous and Biomechanically Compatible Scaffolds for Large-Area Bone Regeneration

Ami R. Amini,[1,2] Douglas J. Adams, Ph.D.,[2] Cato T. Laurencin, M.D., Ph.D.,[1–3] and Syam P. Nukavarapu, Ph.D.[1–3]

Large-area or critical-sized bone defects pose a serious challenge in orthopedic surgery, as all current treatment options present with shortcomings. Bone tissue engineering offers a more promising alternative treatment strategy. However, this approach requires mechanically stable scaffolds that support homogenous bone formation throughout the scaffold thickness. Despite advances in scaffold fabrication, current scaffold-based techniques are unable to support uniform, three-dimensional bone regeneration, and are limited to only the scaffold surface *in vitro* and *in vivo*. This is mainly because of inadequate scaffold pore sizes ($<200\,\mu m$) and accessible pore volume, and the associated limited oxygen diffusion and vascular invasion. In this study, we have adopted a method combining microsphere-sintering and porogen-leaching techniques to fabricate scaffolds with an increased accessible pore volume. Of the scaffolds developed, moderately porous poly(85 lactide-co-15 glycolide) (PLGA) microsphere scaffolds were selected as most advantageous, since they retain mechanical strength in the range of human cancellous bone and display a significantly higher accessible pore volume, which is attributed to an increased percentage of larger pores (i.e., size range 200–600 μm). Unlike control scaffolds with a limited pore size and an accessible pore volume, moderately porous scaffolds displayed increased oxygen diffusion, pre-osteoblast cell infiltration, proliferation, and survival throughout the entire scaffold. Furthermore, moderately porous PLGA microsphere scaffolds displayed enhanced and homogenous mineralization *in vitro*. Since these newly designed moderately porous scaffolds are weight bearing, are fully osteoconductive, and have the ability to support vascularization, they may serve as effective scaffolds for large-area bone defect repair/regeneration. In addition, this study demonstrates the ability to modulate scaffold porosity and, in turn, to develop oxygen tension-controlled matrices that are effective for large-area bone regeneration.

Introduction

Large-area or critical-sized bone defects remain a major clinical problem in orthopedic surgery and cranio-/maxillo-facial surgery, and contribute to the $2.5 billion bone grafting market in the United States.[1] Large-area bone defects may result from trauma, tumor resection, revision surgery, and developmental deformities, and are unable to heal spontaneously.[2] Repair of large defects require bone grafts/graft substitutes that can physically support bone regeneration, while providing the surface area for cell attachment and tissue growth. Current treatment options for large-area bone defects include bone grafts, distraction osteogenesis, demineralized bone matrix, and porous hydroxyapatite—all of which have been associated with significant challenges and complications.[3–8] Thus, there is a warranted search for better bone replacement methods to overcome the drawbacks of the currently used bone graft materials.

Bone tissue engineering (BTE) has been proposed as a more effective alternative option for bone defect repair/regeneration. BTE involves the combination of biodegradable and porous scaffolds, with or without the use of bone-forming cells and growth factors, to regenerate bone.[9–11] The success of the scaffold-based bone regeneration approach critically depends on the effectiveness of the biodegradable scaffold.[12] Important design considerations for BTE scaffolds include biocompatibility, mechanical compatibility, osteoconductivity (i.e., the ability of bone cells to grow on scaffold surface and form bone), osteoinductivity (i.e., the ability to recruit and stimulate differentiation of progenitor cells into osteoblasts), and osteointegration (i.e., the ability to achieve direct bone-to-implant contact).[13] Of these, osteoconductivity of a scaffold is critical, because cell survival and proliferation in the scaffold's interior rely on mass transport upon initial implantation until the onset of vascular invasion.[14]

[1]Institute for Regenerative Engineering and [2]Department of Orthopaedic Surgery, University of Connecticut Health Center, Farmington, Connecticut.
[3]Chemical, Materials and Biomolecular Engineering, University of Connecticut, Storrs, Connecticut.

Methods to achieve cellular conduction involve scaffold pore-structure optimization.[15–17] Scaffolds currently designed with a decreased accessible volume and/or small pore sizes (i.e., $<200\,\mu m$) display osteoblast survival and bone formation limited to the periphery, owing to decreased oxygen and nutrient diffusion throughout the scaffolds.[17] On the other hand, studies have demonstrated that scaffolds with increased accessible volume and/or large pore sizes (i.e., macroporous, $>200\,\mu m$) display increased osteoblast proliferation and differentiation throughout the entire scaffold, as a result of enhanced mass transport of oxygen and nutrients, and neovascularization.[18–20] There have been many efforts to improve scaffold's overall osteoconductivity by fabricating macroporous scaffolds that support osteoblast survival and growth throughout the scaffold. Various scaffolding methodologies have been utilized to fabricate macroporous scaffolds, including gas foaming,[21] freeze drying,[22,23] phase separation,[24,25] and porogen leaching.[26–29] However, in comparison to scaffolds with smaller pore sizes, these macroporous scaffolds display a significant decrease in mechanical strength. For instance, Martin *et al.* demonstrated that poly(85 lactide-co-15 glycolide) (PLGA) foam scaffolds display uniform mineralization throughout, but have inferior mechanical strength (i.e., average compressive modulus of 1.3 MPa).[30] Therefore, there is a clinical need to develop biodegradable scaffolds with optimal pore characteristics and adequate mechanical strength required to support large-area bone regeneration.

PLGA microsphere scaffolds have attracted much attention for BTE, because they display human cancellous bone-compatible mechanical properties and have demonstrated bone formation *in vivo*.[31,32] However, the current PLGA microsphere scaffolds, like other scaffold types with limited accessible volume and pore sizes, fail to provide the prerequisites for optimal bone regeneration (i.e., a stable oxygen and nutrient supply), limiting bone regeneration only to the scaffold surfaces.[17,33] Although Boschetti *et al.* have reported the fabrication of mechanically stable macroporous microsphere scaffolds, this study included only preliminary cellular biocompatibility studies using fibroblasts.[34] In the present study, we systematically examined a novel set of PLGA microsphere scaffolds using pre-osteoblastic cells, and performed comprehensive analyses on the effects of increased porosity and oxygen tension in respect to cell seeding, proliferation, survival, and mineralization. Through this study, we established optimally porous, biodegradable scaffolds that are load bearing, fully osteoconductive, and suitable for large-area bone defect repair.

Materials and Methods

Microsphere fabrication

PLGA microspheres were prepared by an oil-in-water method as reported previously.[31,35] In brief, PLGA 85/15 (Lakeshore Biomaterials) was dissolved in methylene chloride (L-14119; Fisher Scientific) in a 1:5 dilution ratio (i.e., 4 g PLGA:20 mL of methylene chloride). The PLGA/methylene chloride solution was added slowly to 1 L of the 1% polyvinyl alcohol (Sigma-Aldrich) solution under a stirring speed of 250 RPM. The stirring continued for 24 h to allow the methylene chloride to evaporate. The resultant PLGA microspheres were washed with distilled water, filtered, air-dried, sieved into different sizes, and stored in a desiccator until further use.

Scaffold fabrication via thermal sintering and porogen leaching

A new scaffolding method of thermal sintering and porogen leaching developed in this study was used to fabricate microsphere scaffolds with increased porosity. A schematic illustration of this method is shown in Figure 1a. In brief, PLGA microspheres (diameter 425–600 μm) and a porogen, NaCl (diameter 200–300 μm), were mixed at specific weight ratios (i.e., PLGA:NaCl ratios of 100:0, 90:10, 80:20, 70:30, 60:40, and 50:50). The PLGA/NaCl mixture was then placed into a steel mold and thermally sintered at 100°C. The NaCl porogen was leached out by soaking the composite PLGA/NaCl scaffolds in distilled water for 2 h, resulting in scaffolds with increased porosity compared to control scaffolds. The scaffolds with 0% NaCl are referred to

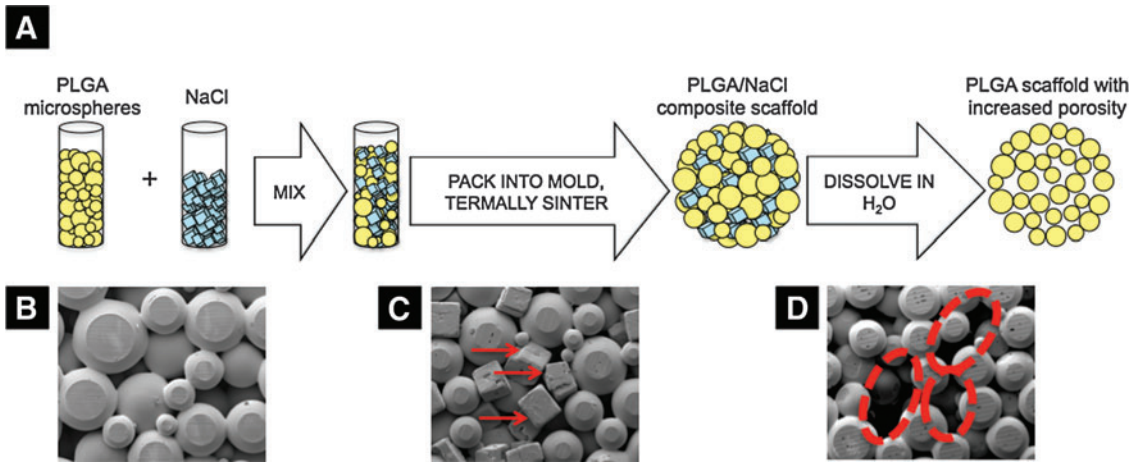

FIG. 1. **(A)** Schematic diagram illustrating the fabrication process of poly(85 lactide-co-15 glycolide) (PLGA) microsphere scaffolds with increased porosity. The scanning electron microscopic image of **(B)** PLGA microspheres after thermal sintering, **(C)** PLGA/NaCl composite scaffold after sintering (red arrows indicate NaCl crystals), and **(D)** PLGA scaffold with increased porosity created after thermal sintering followed by porogen leaching (red dotted circles highlight increased pore sizes). Color images available online at www.liebertonline.com/tea

as control PLGA scaffolds, while the rest as macroporous scaffolds. We fabricated disc-shaped scaffolds (10-mm diameter and 2-mm height) for porosity measurements and the majority of cellular studies, and cylinder-shaped scaffolds (5-mm diameter and 10-mm height) for mechanical testing, live-dead study, and part of mineralization studies. Scaffolds were air-dried and stored in a desiccator until future use. Scanning electron microscopy (SEM) was used to image the morphology of the microsphere scaffolds and to visually examine the increased number of large pore sizes after NaCl leaching.

Evaluation of scaffold porosity

Scaffold specimens were imaged using cone-beam microfocus X-ray computed tomography (CT) to render three-dimensional (3D) models for direct quantitation of porosity (μCT40; Scanco Medical AG). Serial tomographic images were acquired at 45 kV and 177 μA, collecting 2000 projections per rotation at 300 ms integration time. Three-dimensional 16-bit grayscale images were reconstructed using standard convolution back-projection algorithms with Shepp and Logan filtering, and rendered within a 12.3-mm field of view at a discrete density of 4,629,630 voxels/mm^3 (isometric 6 μm voxels). Segmentation of solid scaffold from open porosity was performed in conjunction with a constrained Gaussian filter to reduce noise, applying a threshold of −220 Hounsfield units (water = 0, air = −1000). Direct measurements of internal porosity included volume fraction, size, connectivity, accessible internal pore volume, and accessible solid surface area of the scaffold (as a function of pore dimension). The accessible volume and surface parameters provide direct measurements of the pore volume and the surface available to cell infiltration as a function of minimum pore dimension, using a distance transformation algorithm similar to Moore *et al*'s.[36]

Mechanical testing of PLGA microsphere scaffolds

Compressive testing of cylindrical PLGA microsphere scaffolds (5-mm diameter × 10-mm height, $n = 6$/group) was performed at 2 mm/min (model 5544; Instron Corp.) following the standard protocol of ASTM 1621.[37] Compressive strength was defined as the maximum stress magnitude. Apparent modulus was measured as the tangential slope of the linear region of the effective stress–strain curve at 50% of compressive strength magnitude.

MC3T3-E1 pre-osteoblast cell culture

The pre-osteoblast immortalized cell line MC3T3-E1 (American Type Culture Collection, Manassas, VA) was cultured in an α-minimal essential medium (α-MEM) containing 10% fetal bovine serum (FBS) and 1% penicillin/streptomycin at 37°C, 5% CO_2, and 95% humidified air. Cells were maintained in sub-confluent cultures until needed for *in vitro* scaffold studies.

Cell seeding and culture on scaffolds

PLGA microsphere scaffolds were sterilized by immersing the scaffolds in 70% ethanol for 20 min. Scaffolds were then washed three times in sterile phosphate-buffered saline (PBS) before exposing them to ultraviolet radiation for 1 h. After cell trypsinization, an MC3T3 cell suspension containing 4×10^4 cells was uniformly seeded onto the scaffolds. The disc-shaped scaffolds were placed flat on the culture plate, and a 20-μL cell suspension was uniformly added to the top of the scaffold. The cylindrical scaffolds were placed along the length of the scaffold on the culture plate, and a 40-μL cell suspension was added to the lengthwise surface as the scaffold was slowly rotated (i.e., along the long axis of the scaffold) to maintain uniform cell seeding. The cell-seeded scaffolds were incubated for 2 h at 37°C to allow for cell adhesion onto the scaffolds. The cell–scaffold constructs were cultured in osteogenic media (i.e., α-MEM supplemented with 10% FBS, 1% penicillin/streptomycin, 3 mM β-glycerophosphate, and 50 μg/mL ascorbic acid), and maintained for 7, 14, 21, and 28 days in an incubator at 37°C, 5% CO_2, and 95% humidified air.

Cell-seeding efficiency

After 6 h of cell seeding, scaffolds were transferred to new wells. Cells at the bottom of the original wells were trypsinized, resuspended, and counted with a hemocytometer. The cell-seeding efficiency (i.e., the number of cells that adhered to the scaffolds) was determined by the difference between the number of cells initially seeded (i.e., 4×10^4 cells) and the number of cells that were counted at the bottom of the well.

Cell proliferation on scaffolds

DNA concentration of the pre-osteoblast MC3T3 cells cultured on control PLGA scaffolds and PLGA scaffolds with increased porosity ($n = 3$) was evaluated quantitatively using the Quant-iT PicoGreen dsDNA assay (Invitrogen) following manufacturer's instructions. After culturing the samples (scaffold dimensions 8-mm diameter × 2-mm height) for 7, 14, and 21 days in osteogenic media, the cell–scaffold samples ($n = 3$) for each experimental group were harvested. Samples were washed with PBS, incubated in lysis buffer (i.e., 1% Triton X-100 solution), and subjected to freeze–thaw cycles. The DNA concentration from the cell lysates was determined according to the manufacturer's protocol. Experimental groups included control scaffolds (i.e., 0:100 ratio of NaCl:PLGA) and scaffolds with increased porosity (i.e., 10:90, 20:80, 30:70, and 40:60 ratio of NaCl:PLGA).

Cell viability on surface and interior of scaffolds

The live-dead cell viability assay we used (Invitrogen) includes calcein AM and ethidium homodimer-1 probes to label live and dead cells green and red, respectively. We used this live-dead assay to compare MC3T3 cell survival on the surface and in the interior of scaffolds. Cylindrical scaffolds (5-mm diameter and 10-mm height) were cultured for 4, 7, and 14 days in osteogenic media, the point at which scaffolds ($n = 3$) for each experimental group were harvested. Samples were bisected lengthwise from each scaffold group to allow for the examination of cell viability in the sample's interior. The live-dead cell viability assay was performed according to the manufacturer's protocol, using confocal microscopy to image cells at the surface and interior of the scaffolds.

Cell localization and expression

To visualize cellular localization and expression via histology and immunohistochemistry, samples were paraffin-

embedded and sectioned.[38] Briefly, cell–scaffold constructs were washed with PBS, and then fixed in formalin overnight at 4°C. Samples were dehydrated sequentially using an isopropyl alcohol series (i.e., 70%, 90%, and 100%) for 1 h each, at room temperature. Samples were directly transferred to molten paraffin (Tissue Path Paraplast Tissue Embedding Media; Fisher Scientific) at 55°C for 10 min, and then embedded in fresh molten paraffin. Paraffin-embedded samples were cut into serial sections (20 μm thick) using Cryofilm (Section-Lab Co. Ltd.) and a microtome sectioning machine. Sections were placed on glass slides for histological analysis. Sections were stained with Gill's 3 hematoxylin (Sigma-Aldrich) to visualize MC3T3 cell localization within the PLGA scaffolds after culturing the constructs for 28 days in osteogenic media. Immunostaining of two bone markers, osteopontin (OPN) and collagen type I (Col I), was performed via a rabbit polyclonal anti-human OPN (Abcam; ab8448) antibody and a rabbit polyclonal anti-human Col I antibody (Abcam; ab292), respectively. Briefly, sections were de-paraffinized in HistoClear (National Diagnostics), taken through a descending series of ethanol concentrations, rehydrated in distilled water, and then placed in 3% hydrogen peroxide (Sigma-Aldrich) in PBS to quench endogenous peroxidase activity. To improve antigen exposure, the sections were boiled in Target retrieval (Dako) and washed in distilled water. Samples were incubated with blocking solution (i.e., 0.5% [w/v] bovine serum albumin in PBS) for 1 h. Primary antibodies were diluted in 0.5% (w/v) bovine serum albumin in PBS at concentrations of 1:200 for OPN or 1:300 for Col I. Samples were incubated with the primary antibody for 2 h at room temperature. Sections were washed free of the primary antibody and incubated with the SignalStain® Boost IHC Detection Reagent, HRP, Rabbit (Cell Signaling; #8114) followed by an incubation with 3,3′-diaminobenzidine (Vector Laboratories) for 30 s. The slides were rinsed three times in water, and mounted using mounting media (Electron Microscopy Sciences) for 30 min.

Scaffold mineralization potential

Matrix mineralization or calcium deposition was evaluated via alizarin red staining. This colorimetric analysis is based on solubility of the red-matrix precipitate with cetylpyridinium chloride (CPC; Sigma-Aldrich) to yield a purple solution. Briefly, after 14, 21, and 28 days of culturing in osteogenic media, cell–scaffold constructs were washed with distilled water and fixed with 70% ethanol at 4°C for 1 h. Ethanol was removed and samples were air-dried for 10 min. Samples were incubated with the alizarin red dye (Sigma-Aldrich) for 10 min at room temperature. After washing the samples to remove the excess of alizarin red dye, the samples were incubated with 10% CPC at room temperature for 30 min. The absorbance of the resulting solution, which is proportional to the amount of calcium deposited, was read on a TECAN plate reader at 562 nm.

Oxygen tension measurements

After culturing the MC3T3-E1 cells on control and macroporous PLGA scaffolds for 21 days in osteogenic media, the cell–scaffold samples were quantitatively evaluated for the oxygen tension in the interior region of each sample group using needle-type fiber-optic oxygen microsensors (501656; World Precision), as previously described by Volkmer *et al.*[20] Specifically, we examined scaffold groups with 0%, 10%, 20%, 30%, and 40% NaCl, and cultured 100,000 cells on each scaffold (dimensions 5-mm diameter and 10-mm height). The oxygen sensors were mounted on optic fibers with a tip diameter of 50 μm. To protect these fragile sensors, they are fixed within a standard hollow 27-gauge needle of 0.4-mm diameter. A 25-gauge needle was utilized to pre-form a 2.5-mm-deep channel on the side of the scaffold for which the probe would then be inserted (305127; Becton Dickinson). Oxygen tension measurements in the medium were taken by inserting a probe in the medium next to all experimental scaffold groups. Before sample measurements, the oxygen microsensor was calibrated following a conventional two-point calibration protocol described by the manufacturer. Briefly, oxygen-free water and water-vapor-saturated air were used as calibration standards. The oxygen-free water standard was prepared by dissolving 1 g of sodium sulfite (S430; Fisher Scientific) in 100 mL of water in a sealed vessel, and the water-vapor-saturated air was prepared by placing a wet piece of cotton in a sealed vessel. The oxygen tension measurements are expressed as the mean of three samples per scaffold group ± standard deviation (SD).

Statistical analysis

For cell-seeding efficiency, cell proliferation, and mineralization assays, a two-way analysis of variance was preformed to compare data. Three scaffolds per group were analyzed at each time point. Error is reported in figures as the SD, and significance was determined using a probability value of $p < 0.050$.

Results

Microsphere scaffolds with increased porosity

PLGA microsphere sintering often results in 3D scaffolds with limited pore volume. However, we developed a novel method to fabricate PLGA microsphere scaffolds with increased pore volume and an average pore size, as shown in Figure 1A. Through mixing a porogen (i.e., NaCl crystals, 200–300 μm diameter) with PLGA microspheres (425–600 μm diameter), thermal sintering, and porogen leaching, we successfully created PLGA microsphere scaffolds with an increased pore volume. Thermal sintering and particulate leaching are well-known methods for fabricating 3D and porous scaffolds.[26,31] Here, we combined them into a single-method Thermal Sintering and Porogen Leaching to design PLGA microsphere scaffolds with the desired pore characteristics. SEM imaging demonstrated that after porogen leaching (Fig. 1D), there was visually an increase in the number of large pore sizes compared to scaffolds fabricated with PLGA microspheres alone (i.e., control PLGA scaffolds).

Scaffold porosity via micro-CT

Micro-CT imaging was used to reconstruct 3D models of scaffolds for nondestructive measurements of porosity. Computational assessment of all micro-CT images confirmed that the internal porosity is an interconnected space comprising 99.9% of the total pore volume. The porosity and accessible volume of the PLGA microsphere scaffolds

corresponded to the porogen size and to the amount used. For example, by mixing 40% NaCl and 60% PLGA microspheres (by dry weight), percent accessible pore volume increased 337% in relation to control scaffolds at an average pore size of 200 μm (Fig. 2B). Data and images describing scaffold pore volume are presented as a function of pore size, providing direct measurements of an externally accessible pore space through the full range of the diametral pore dimension (Fig. 2A, C). Although the range of pore size dimensions remained constant, the volume of porosity increased with higher concentration of porogen. For example, blue areas signify the accessible volume in the scaffolds to objects with a diameter in the range of 100–200 μm, and red areas in the range of 400–500 μm. Thus, as the porogen concentration increased, the accessible interconnected volume also increased (Fig. 2A). In control scaffolds, a sphere with a diameter of 200 μm can access ~10% of the total pore volume, whereas the same sphere can access ~40% of the pore volume of the 40% NaCl/60% PLGA scaffold. This is illustrated in Figure 2C, which again shows that the experimental scaffolds fabricated with a porogen have a higher percentage of accessible pore volume in the 300–500 μm range in comparison to the control scaffold. Thus, we effectively increased the accessible volume for cell infiltration throughout the scaffold.

Scaffold mechanical characterization

By using an increasing amount of porogen in the scaffold fabrication process, compressive strength and modulus of the scaffolds were sacrificed (Fig. 3). Scaffolds with increased porosity (i.e., 40% NaCl/60% PLGA by dry weight) displayed significantly less compressive strength and modulus than control scaffolds (i.e., 0% NaCl/100% PLGA). Scaffolds with moderately sized pores (i.e., 20% NaCl/80% PLGA) displayed a significant decrease, 63.2%, in compressive strength, and a 29.8% decrease in compressive modulus in comparison to control scaffolds. The 20% NaCl/80% PLGA displayed significantly higher compressive strength, 140%, and modulus, 240%, than scaffolds with the highest porosity

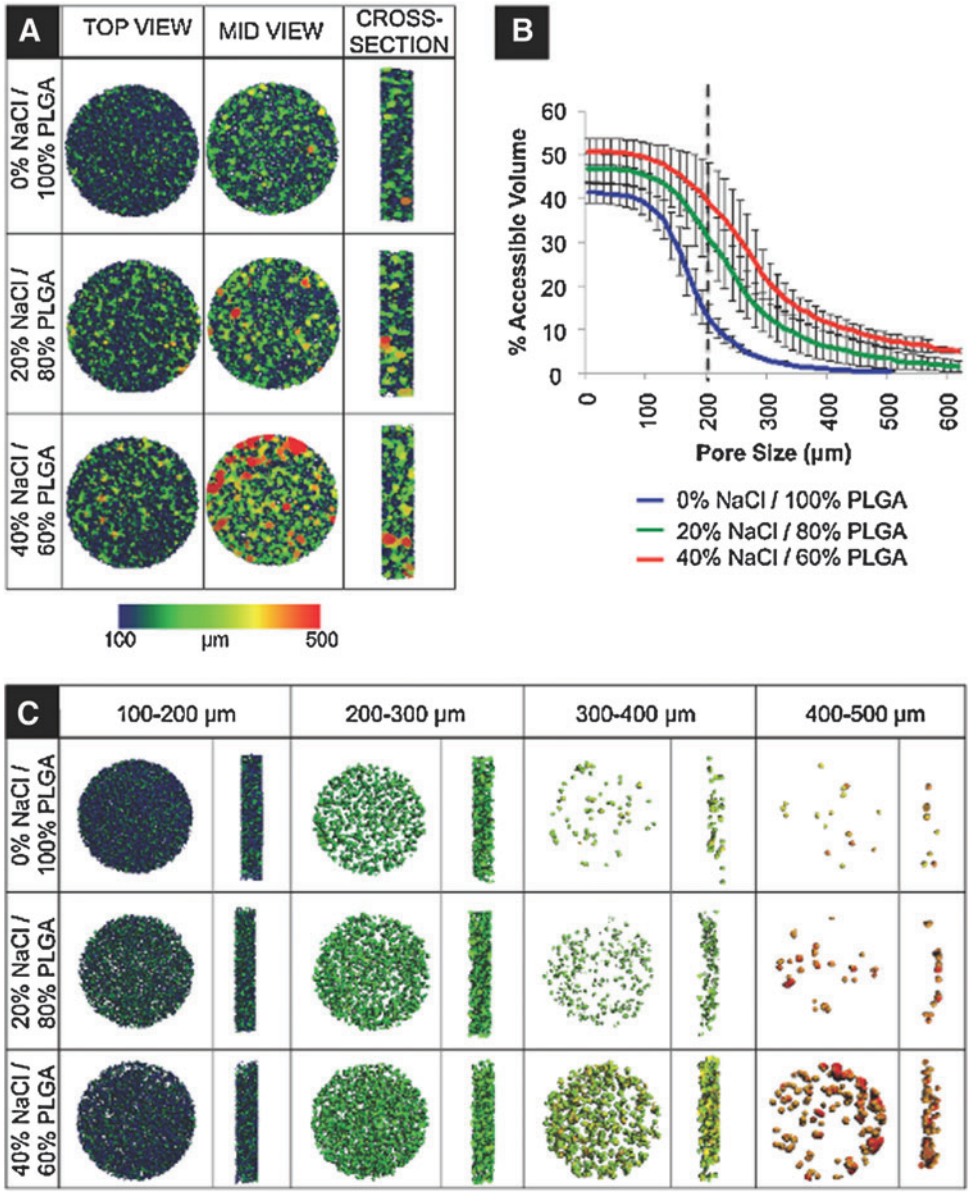

FIG. 2. Scaffold pore interconnectivity and percent accessible volume obtained via micro-computed tomography imaging and analysis. **(A)** Accessible volume images generated by imposing specific pore diameter parameters (scale 100–500 μm) on 0% NaCl/100% PLGA, 20% NaCl/80% PLGA, and 40% NaCl/60% PLGA scaffolds from a top-view, mid-view, and cross-sectional view. **(B)** Graph comparing the effect of increasing porogen to accessible volume in the PLGA scaffolds. Dashed line illustrates percent accessible volume of PLGA/0% NaCl and PLGA/40% NaCl scaffolds for an object with a diameter of 200 μm. **(C)** Increasing scaffold accessible volume in moderately porous PLGA scaffolds. Interconnected volume accessible to spherical objects with a specific diameter range (i.e., 100–200, 200–300, 300–400, and 400–500 μm) in PLGA/0% NaCl, PLGA/20% NaCl, and PLGA/40% NaCl scaffolds. Color images available online at www.liebertonline.com/tea

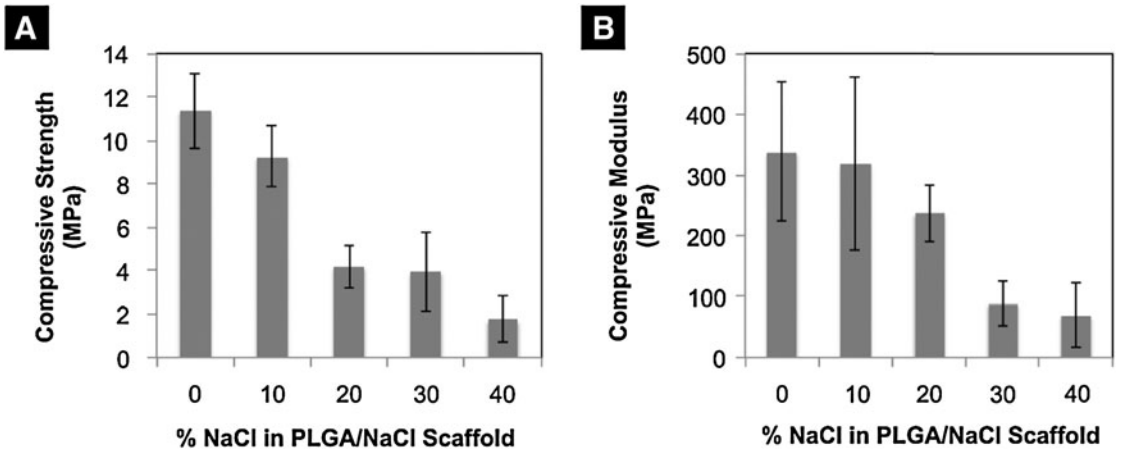

FIG. 3. Mechanical characterization of PLGA microsphere scaffolds with an increased porogen content. Analysis of **(A)** compressive strength and **(B)** compressive modulus.

(i.e., 40% NaCl/60% PLGA). The compressive modulus and strength for the scaffolds with increased porosity (i.e., scaffolds fabricated with greater than 10% NaCl), although lower than the control scaffold, are in the range of human trabecular bone mechanical properties (i.e., compressive modulus 50–800 MPa and compressive strength 1–10 MPa).[39] Thus, we termed the 20% NaCl/80% PLGA scaffolds as moderately porous scaffolds, since they display significantly a higher pore volume than control, while retaining their mechanical strength.

Effect of the scaffold-accessible pore volume on pre-osteoblast cell infiltration, proliferation, and survival

The efficiency of initial cell seeding decreased in scaffolds that were fabricated with NaCl (Fig. 4). Of the 4×10^4 MC3T3 cells initially seeded onto each scaffold, $\sim3.3\times10^4$ cells adhered to the control scaffolds, and only 2.5×10^4 cells adhered to the scaffolds with increased porosity (i.e., 40% NaCl/60% PLGA by dry weight). However, after 5 days of culture in osteogenic media, the DNA concentration, which is proportional to cell number, was not significantly different in control scaffolds and in scaffolds with increased porosity (i.e., 20% NaCl/80% PLGA and 40% NaCl/60% PLGA by dry weight). By 2 weeks of culture, the cell number and proliferation in the scaffolds with increased porosity exceeded that of control scaffolds (Fig. 5). The limitation of cell culture on scaffolds was seen by 3 weeks of culture, as the capacity of the scaffolds to support cell proliferation began to decrease. The effects of scaffold porosity on cell viability were examined on the surface of the scaffolds as well as in the interior of the scaffolds. At 4, 7, and 14 days of cultures, cell–scaffold constructs were bisected, and live/dead assays were performed. Representative fields from the center of the scaffold ($\sim$5-mm depth) taken by a confocal microscopy are shown in Figure 6. After 4 days of culture, there was not a significant difference in live:dead cell ratio between the control scaffolds and scaffolds with increased porosity. By 14 days of culture, we observed a significant difference in live cells present in the interior region of scaffolds with increased porosity versus control scaffolds. In 20% NaCl/80% PLGA and 40% NaCl/60% PLGA scaffolds, the cells displayed a robust and healthy morphology, with extended processes. In contrast, the cells in the center of the control scaffolds were mostly dead by 14 days and displayed a round morphology.

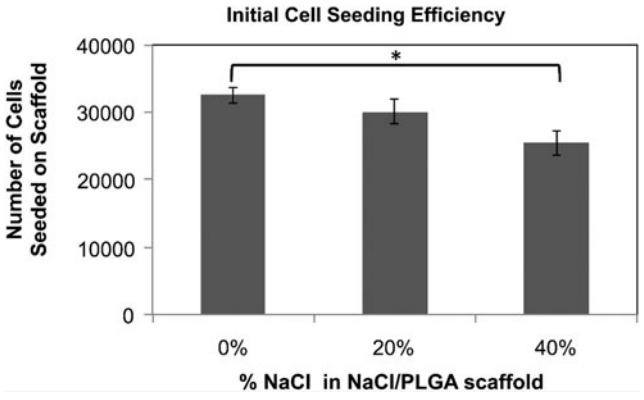

FIG. 4. Effect of increasing porosity on cell-seeding efficiency on scaffolds ($^*p<0.05$).

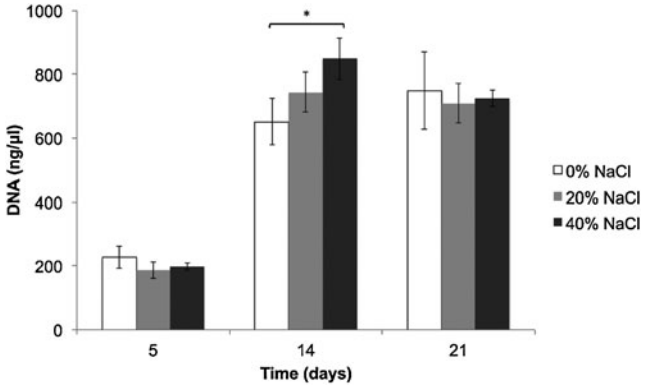

FIG. 5. Effect of increasing porosity on proliferation of murine pre-osteoblast cells (MC3T3-E1) seeded on PLGA control and moderately porous scaffolds at 5, 14, and 21 days ($^*p<0.05$).

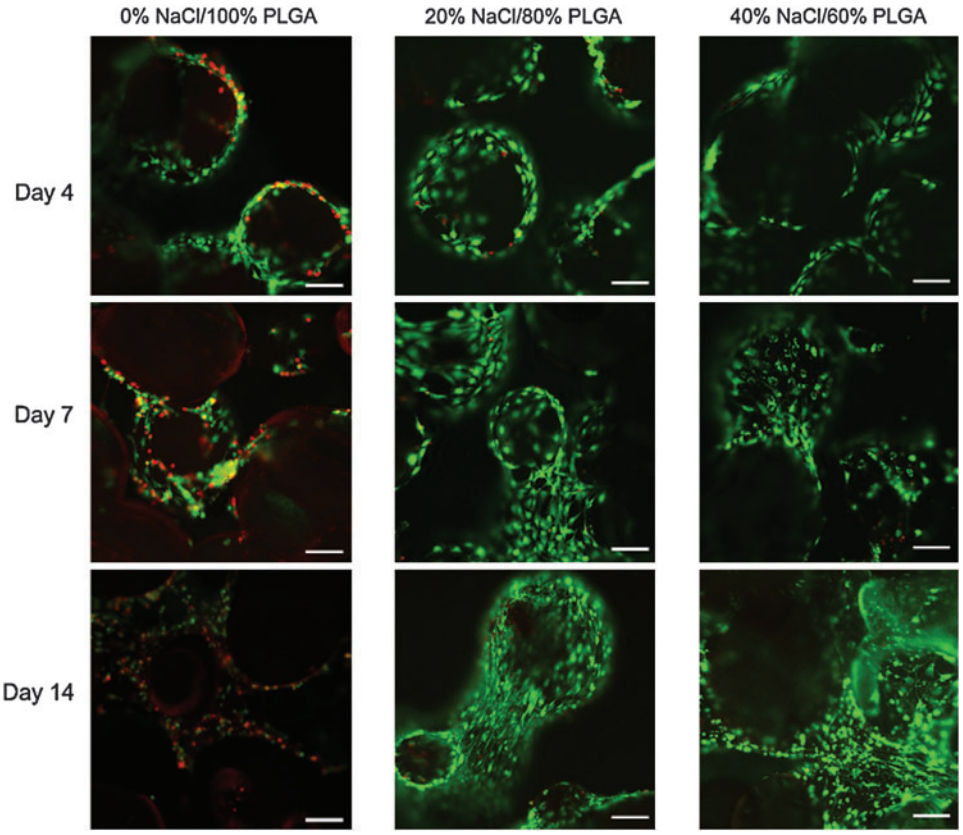

FIG. 6. Effect of increasing porosity on cell viability in the interior of the PLGA microsphere scaffolds at 4, 7, and 14 days (scale = 200 μm). Color images available online at www.liebertonline.com/tea

Cell localization and expression on PLGA microsphere scaffolds

Through a modified paraffin-embedding and sectioning procedure, as described in the Cell localization and expression section, we were able to study cellular localization and expression of the MC3T3 cells cultured on our PLGA microsphere scaffolds. In Figure 7, PLGA scaffolds with increasing porosity (i.e., 20% NaCl/80% PLGA and 40% NaCl/60% PLGA; images of 40% NaCl/60% PLGA scaffolds are not shown) promote cell infiltration into the interior of the scaffolds. After 28 days of culturing MC3T3 cells on the scaffolds, hematoxylin staining highlighted cells that are densely located on the top of control scaffolds and not in the center of the control scaffolds (Fig. 7A). On the other hand, scaffolds with increased porosity displayed cell localization on the surface, as well as increased cell infiltration and survival in the center of the scaffold (Fig. 7B, C). Likewise, we found cells expressing OPN and Col I only on the surface of the control scaffolds (Fig. 7D, G). PLGA scaffolds with increased porosity displayed cells expressing OPN and Col I at the top, as well as in the center of the scaffold (Fig. 7E, F, H, I).

Effect of scaffold porosity on mineralization

After 28 days, following seeding and culturing MC3T3 cells on scaffolds, we performed alizarin red staining to detect calcium mineralization. Scaffolds with increased porosity visually appeared to have a higher mineralization potential than control scaffolds (Fig. 8). Control scaffolds displayed mineralization that is limited to the top surface, and not in the center and bottom. On the other hand, scaffolds with increased porosity showed alizarin red staining throughout the entire scaffold (i.e., top and bottom surfaces, and middle of construct). To compare and quantify the mineralization that was occurring throughout the scaffolds versus mineralization occurring only in the center of the scaffolds, we cultured MC3T3 cells on cylindrical scaffolds that were taller (scaffold size 10-mm height and 5-mm diameter), so that we were able to manually dissect 2 mm off the top and bottom scaffold surfaces (Fig. 9). Alizarin red staining quantification confirmed the increase in mineralization in scaffolds with increasing porosity. The 20% NaCl/80% PLGA scaffolds displayed the highest significant difference in mineralization compared to control. Although mineralization in 40% NaCl/60% PLGA scaffolds displayed a higher mineralization potential than in control scaffolds, it was not as high as 20% NaCl/80% PLGA (Fig. 9A). After manually removing the top 2-mm and bottom 2-mm surfaces of the tall cylindrical scaffolds, we quantified the mineralization in the center portions of the scaffolds. Mineralization increased significantly in the center of the scaffolds with increasing porosity after 28 days in culture (Fig. 9B).

Effect of scaffold porosity on oxygen levels in scaffold's interior

Oxygen tension measurements demonstrated a significant gradient between the media surrounding the cultured constructs and the interior regions of the constructs in all experimental groups after 3 weeks *in vitro*. Oxygen tension in the peri-construct region for all experimental scaffold groups was not statistically different from each other, and averaged

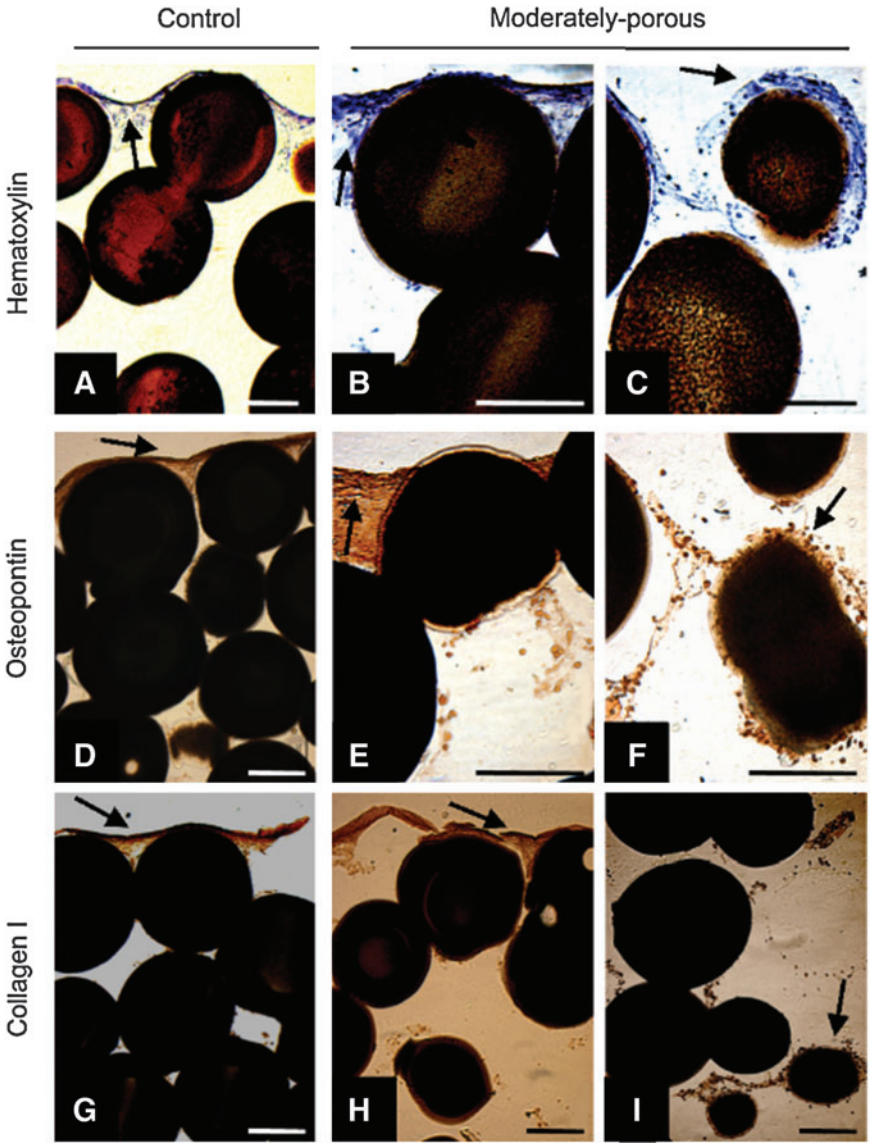

FIG. 7. MC3T3-E1 cellular localization and expression on control and moderately porous PLGA scaffolds. Hematoxylin staining of control **(A)** and moderately porous scaffolds [top **(B)** and center **(C)**], osteopontin immunohistochemistry of control **(D)** moderately porous scaffolds [top **(E)** and center **(F)**], and collagen type I immunohistochemistry of control **(G)** and moderately porous scaffolds [top **(H)** and center **(I)**]. Arrows indicate cell staining. Scale on all images = 200 μm. Color images available online at www.liebertonline.com/tea

6.67% ± 1.11%. Oxygen tension in the interior of the cell-seeded scaffolds was directly related to the concentration of the porogen used to fabricate the scaffolds. Specifically, increase in the scaffold's porosity facilitated and enhanced oxygen diffusion to the construct's interior region, and thus decreasing the oxygen tension gradient from the scaffold's exterior to interior (Fig. 10). The peri-construct–interior construct oxygen gradient was most significantly seen in control scaffolds, where the oxygen gradient in the interior of cell-seeded control (0% NaCl/100% PLGA scaffolds) scaffold conditions dropped below 1%. Moderately porous scaffolds (20% NaCl/80% PLGA scaffolds) displayed similar oxygen tension gradients compared to macroporous scaffolds (40% NaCl/60% PLGA scaffolds).

Discussion

Large-area or critical-sized bone defect repair via scaffold-based BTE requires a mechanically stable scaffold that supports osteogenesis entirely. For this, it is critical to develop a scaffold that allows for oxygen diffusion, and thus cell survival and proliferation in the scaffold's interior regions. In the present study, we have developed a novel biodegradable scaffold for bone regeneration that encompasses the previously mentioned requirements, and demonstrated their ability to promote uniform osteogenesis *in vitro*.

Appropriate scaffold porosity and accessible volume are critical for obtaining effective osteogenesis in large-area bone repair. As seen in Figure 11, deviations from the moderate porosity range display positive and negative tradeoffs. Scaffolds with decreased average pore size are associated with an increase in the surface area, and thus cell-seeding efficiency. Such scaffolds with relatively lower porosity exhibit higher mechanical strength, a critical factor in clinical applications.[40] However, these scaffolds are also associated with significant drawbacks, including decreased mass transport of oxygen and nutrients and decreased vascularization, which in turn, results in decreased osteoblast survival and bone regeneration.[15,17,41,42] On the other hand, scaffolds with high porosity are not as mechanically strong and display decreased cell-seeding efficiency, but are associated with higher mass transport of oxygen and nutrients,

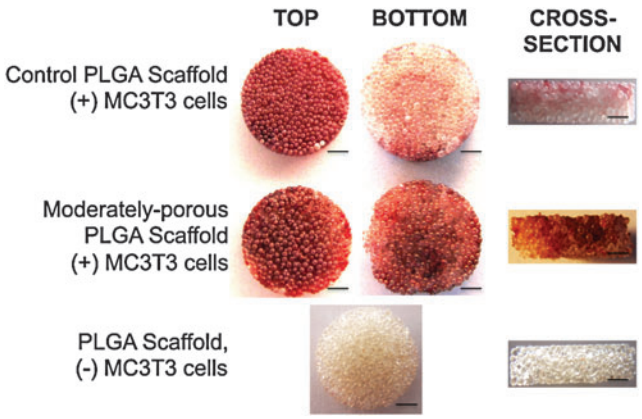

FIG. 8. Mineralization potential of control and moderately porous PLGA microsphere scaffolds. Alizarin red staining was performed 28 days after MC3T3-E1 cells had been cultured on scaffolds. Red staining in images signifies mineralization or calcium deposition. Moderately porous scaffold displayed mineralization on throughout the scaffold (i.e., top and bottom surfaces, and cross section), while control scaffold mineralization is limited to only the top surface of the scaffold. Scale bar = 1000 μm. Color images available online at www.liebertonline.com/tea

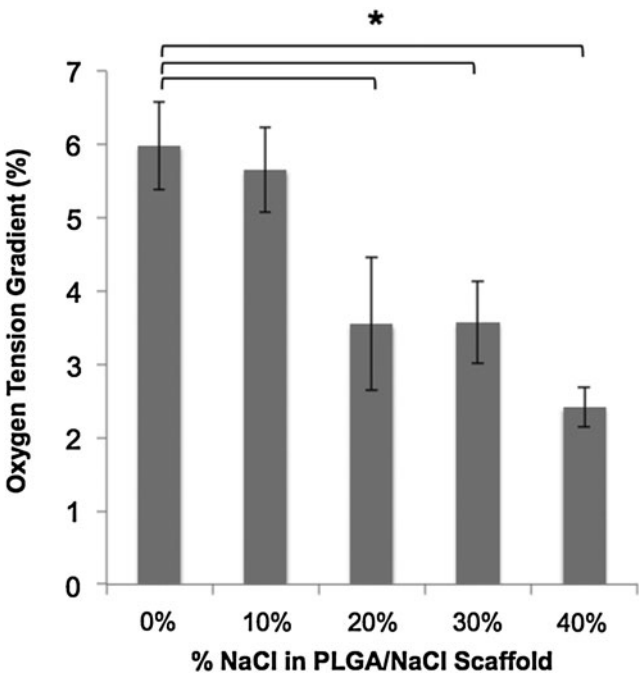

FIG. 10. The effect of porosity on oxygen tension gradient from the exterior to interior of PLGA microsphere scaffolds after 4 weeks *in vitro*. Oxygen tension of ambient air is 21%, and average oxygen tension of cell culture media is 6.67% ± 1.11%.

facilitating enhanced bone regeneration.[43] With respect to dynamic bone remodeling, increased osteoclast number and size in scaffolds with high porosity may result in increased bone matrix strength via increases in bone remodeling.[44] Also, studies have identified scaffolds with increased pore sizes to allow for the most efficient vascularization.[45,46] Thus, scaffold porosity is a crucial parameter to consider when fabricating scaffolds.

For BTE applications, PLGA scaffolds developed via microsphere sintering techniques have a unique advantage, as they display mechanical properties in the range of human cancellous bone,[31] an essential aspect of scaffolds to ensure proper support at the defect site upon implantation. These cancellous-bone, mechanically compatible scaffolds are attractive since the bone has the special ability to undergo remodeling and optimize its mechanical function for its particular skeletal location, and thus can be effectively used for regeneration in either cancellous or cortical bone sites.[47] Our group has fabricated and extensively investigated PLGA 85/15, PLGA–nano hydroxyapatite composites, and PLGA–chitosan-blend microsphere scaffolds for bone regeneration.[31,32,35,48] PLGA 85/15-based microsphere scaffolds have supported bone-forming cell proliferation, differentiation, and mineralization *in vitro*[49,50] and bone formation *in vivo*.[32,33] However, these PLGA microsphere scaffolds lack the necessary porosity for sufficient cell ingrowth, and thus results in surface-limited osteogenesis *in vitro* and *in vivo* (Fig. 12).

To effectively increase microsphere scaffold porosity, we have used microsphere sintering followed by a porogen leaching method. In this method, we combined PLGA microspheres with a porogen (i.e., NaCl particles), thermally sintered, and then leached out the porogen by soaking the constructs in water (Fig. 1). Scaffold porosity and mechanical

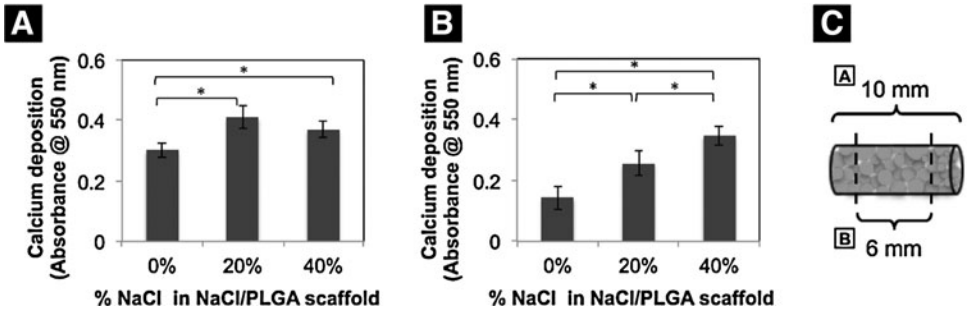

FIG. 9. Effects of porosity on mineralization **(A)** throughout the entire scaffold, and **(B)** in the center of the scaffold. After 28 days of cell culture on scaffolds, alizarin red staining was performed on the entire cell–scaffold construct and quantified. Two millimeters from the top and bottom surfaces of the scaffolds was manually removed as shown in **(C)**, and alizarin red staining was performed to analyze the mineralization in the center of the constructs **(B)** (*$p < 0.05$).

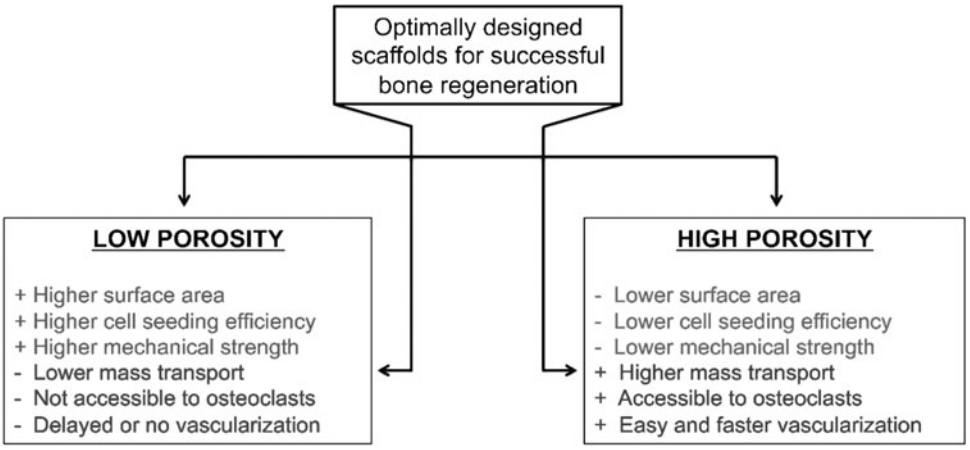

FIG. 11. The pros and cons of scaffolds with low and high porosity, and the requirement to design scaffolds with optimal porosity and mechanical properties (i.e., moderately porous scaffolds) for homogeneous and enhanced bone regeneration.

properties can be tuned according to the clinical requirement by controlling the size and amount of the porogen added during the fabrication process. Through this method, we have improved PLGA microsphere performance and its ability to support osteoblast cell survival, proliferation, and mineralization throughout the construct, and yet retained the mechanical compatibility for effective bone regeneration.

As we increase the dry weight ratio of NaCl:PLGA used during the fabrication process of PLGA microsphere scaffolds, the porosity and accessible volume increases significantly (Table 1). High accessible volume within scaffolds is a crucial parameter that influences the efficiency of nutrient-, gas-, and waste-exchange within the scaffolds, as well as cell migration needed to promote tissue regeneration. Furthermore, it facilitates angiogenesis allowing for blood vessel in-growth, and thus increases the supply of oxygen and nutrients to the center of the construct.[51] However, with increase in pore volume, mechanical integrity is sacrificed (Fig. 3). Scaffolds with a higher ratio of NaCl than that in 40% NaCl/60% PLGA scaffolds were not mechanically stable. Scaffolds fabricated with an intermediate concentration of NaCl (i.e., moderately porous scaffolds; 20% NaCl/80% PLGA scaffolds) were significantly more mechanically robust than those fabricated with 40% NaCl/60% PLGA.

In addition to decreasing mechanical strength, scaffolds with increased porosity display a lower cell-seeding efficiency, as these scaffolds are less efficient in retaining cells during the cell-seeding process (Fig. 4). Despite the decrease in initial cell number seeded on the scaffolds with increased porosity, cell numbers on these scaffolds reached that of control scaffolds by 5 days in culture, and surpassed it by 2 weeks in culture (Fig. 5). Thus, scaffolds with larger porosity have a better potential to support cell proliferation *in vitro*, likely due to uniform oxygen tension and near-neutral pH throughout the entire construct. Increased cell survival and activity (i.e., OPN and Col I expression) were confirmed in the interior of scaffolds with increased porosity, compared to that of control scaffolds over a long-term culture. However, there appears to be an important relationship between the mineralization potential and the surface area of scaffold, since macroporous scaffolds (i.e., 40% NaCl/60% PLGA scaffolds) did not display mineralization as high as moderately porous scaffolds. According to these attributes, moderately porous scaffolds display the highest performance in supporting cell infiltration, proliferation, and mineralization throughout the entire construct *in vitro* (Table 1).

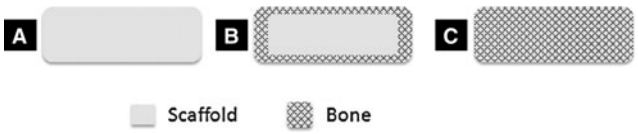

FIG. 12. Schematic illustration of surface-limited and large-area bone regeneration in a biodegradable scaffold. Scaffolds with a limited pore size and reduced oxygen diffusion through their pore structure result in bone cell survival and growth limited to the scaffold surface, and thus surface-limited bone regeneration **(B)**, while optimally porous scaffolds with increased oxygen levels in the scaffold interior allow for bone regeneration throughout the scaffold thickness, which, in turn, can support large-area bone regeneration both *in vitro* and *in vivo* **(C)**. **(A)** is showing the cross-sectional surface of a scaffold.

Our moderately porous scaffolds stand superior to other methods that are currently utilized to increase cell proliferation and mineralization throughout BTE constructs *in vitro*. For instance, bioreactor culture methods are popular alternative methods utilized to increase cell infiltration and proliferation throughout constructs.[52–54] However, unlike bioreactor culture methods, which are complex in nature and only effective *in vitro*, moderately porous-scaffold development is simple and effectively allows for enhanced oxygen tensions throughout the constructs both *in vitro* and *in vivo*. In addition, the increased porosity in moderately porous scaffolds is expected to improve vascularization and osteoclast participation, and hence bone remodeling by closely mimicking the native bone repair process.[44] Lastly, studies have citied a significant enhancement in bone regeneration when adding growth factors (i.e., BMP-2) to BTE constructs.[55–57] However, functional bone regeneration may only occur when the entire construct, including the interior, supports cell survival and proliferation (i.e., fully osteoconductive). The combination of growth factors with an appropriate scaffold, such as our moderately porous scaffold that is fully osteoconductive and may support vascularization throughout, will lead to optimal bone regeneration in large-area bone defects.

In this study, by controlling the scaffold pore size and pore volume, we effectively designed oxygen-tension-controlled

Table 1. Porosity, Mechanical Performance, and Osteoconductivity Comparison Between Control and Moderately Porous Poly (85 Lactide-co-15 Glycolide) Microsphere Scaffolds

	Control scaffold PLGA 85/15	*Moderately porous scaffold (20% NaCl/80% PLGA 85/15)*
Accessible pore volume	~12% pore volume is with pore sizes ≥200 μm	~31% pore volume is with pore sizes ≥200 μm
Mechanical properties		
Compressive modulus	338.4 ± 114.5 MPa	237.4 ± 46.5 MPa
Compressive strength	11.4 ± 1.73 MPa	4.19 ± 0.99 MPa
Cell seeding efficiency	81.3%	63.7%
Cell proliferation	1.87-fold increase from 5 to 14 days *in vitro*	2.98-fold increase from 5 to 14 days *in vitro*
Cell viability and phenotypic expression	Periphery limited	Homogeneous throughout entire scaffold
Mineralization	Surface-limited	Homogeneous throughout entire scaffold (i.e., top, center, and bottom) 35.5% more mineralization in entire scaffold 79.2% more mineralization in scaffold's interior
Osteoconductivity	Surface-limited	Fully osteoconductive
Oxygen% in scaffold interior	0.69% ± 0.60%	3.13% ± 0.91%

PLGA, poly(85 lactide-co-15 glycolide).

matrices. Increasing the amount of porogen resulted in a systematic increase in not only porosity, but also available oxygen tension throughout the matrix. The enhanced survival, proliferation, differentiation, and mineralization of pre-osteoblasts may be attributed to the increase in available oxygen tension. However, this increased cell performance may be cell-type specific, as other cell types, such as chrondrocytes, display enhanced performance in scaffolds with low porosity.[58]

Thus, the proposed moderately porous scaffolds with improved oxygen availability and bone-compatible mechanical properties are desirable for large-area bone regeneration. Oxygen tension control via scaffold porosity optimization may provide opportunities in designing next-generation scaffold systems most effective for large-area or critical-sized bone defect repair.

Acknowledgments

Dr. Nukavarapu would like to acknowledge funding from the University of Connecticut through the Inter Campus Incentive Grant Program. The authors thank funding from the Institute for Regenerative Engineering (IRE), the University of Connecticut. The authors also acknowledge Vilmaris Diaz-Doran for her assistance with the micro-CT work, Ashley Amini for her help with confocal microscopy, and Paiyz Mikael for her help with SEM.

Disclosure Statement

No competing financial interests exist.

References

1. Laurencin, C., Khan, Y., and El-Amin, S.F. Bone graft substitutes. Expert Rev Med Dev **3,** 49, 2006.
2. Pneumaticos, S.G., Triantafyllopoulos, G.K., Basdra, E.K., and Papavassiliou, A.G. Segmental bone defects: from cellular and molecular pathways to the development of novel biological treatments. J Cell Mol Med **14,** 2561, 2010.
3. Tomford, W.W., Starkweather, R.J., and Goldman, M.H. A study of the clinical incidence of infection in the use of banked allograft bone. J Bone Joint Surg Am **63,** 244, 1981.
4. Lord, C.F., Gebhardt, M.C., Tomford, W.W., and Mankin, H.J. Infection in bone allografts. Incidence, nature, and treatment. J Bone Joint Surg Am **70,** 369, 1988.
5. Gazdag, A.R., Lane, J.M., Glaser, D., and Forster, R.A. Alternatives to autogenous bone graft: efficacy and indications. J Am Acad Orthop Surg **3,** 1, 1995.
6. Banwart, J.C., Asher, M.A., and Hassanein, R.S. Iliac crest bone graft harvest donor site morbidity. A statistical evaluation. Spine (Phila Pa 1976) **20,** 1055, 1995.
7. Arrington, E.D., Smith, W.J., Chambers, H.G., Bucknell, A.L., and Davino, N.A. Complications of iliac crest bone graft harvesting. Clin Orthop Relat Res 300, 1996.
8. Delloye, C., Cornu, O., Druez, V., and Barbier, O. Bone allografts: what they can offer and what they cannot. J Bone Joint Surg Br **89,** 574, 2007.
9. Langer, R., and Vacanti, J.P. Tissue engineering. Science **260,** 920, 1993.
10. Petite, H., Viateau, V., Bensaïd, W., Meunier, A., de Pollak, C., Bourguignon, M., *et al.* Tissue-engineered bone regeneration. Nat Biotechnol **18,** 959, 2000.
11. Nukavarapu, S.P., Wallace, J., Elgendy, H., Lieberman, J., and Laurencin, C.T. Bone and biomaterials. In: Hollinger, J.O., ed. An Introduction to Biomaterials and Their Applications, 2nd edition. Boca Raton: CRC Press, 2011, pp. 571–593.
12. Hutmacher, D.W. Scaffolds in tissue engineering bone and cartilage. Biomaterials **21,** 2529, 2000.
13. Albrektsson, T., and Johansson, C. Osteoinduction, osteoconduction and osseointegration. Eur Spine J **10 Suppl 2,** S96, 2001.
14. Vaccaro, A.R. The role of the osteoconductive scaffold in synthetic bone graft. Orthopedics **25,** s571, 2002.
15. Tsuruga, E., Takita, H., Itoh, H., Wakisaka, Y., and Kuboki, Y. Pore size of porous hydroxyapatite as the cell-substratum controls BMP-induced osteogenesis. J Biochem **121,** 317, 1997.
16. Kuboki, Y., Jin, Q., and Takita, H. Geometry of carriers controlling phenotypic expression in BMP-induced

osteogenesis and chondrogenesis. J Bone Joint Surg Am **83-A Suppl 1,** S105, 2001.
17. Karageorgiou, V., and Kaplan, D. Porosity of 3D biomaterial scaffolds and osteogenesis. Biomaterials **26,** 5474, 2005.
18. Kühne, J., Bartl, R., Frisch, B., Hammer, C., Jansson, V., and Zimmer, M. Bone formation in coralline hydroxyapatite. Effects of pore size studied in rabbits. Acta Orthop Scand **65,** 246, 1994.
19. Holtorf, H.L., Datta, N., Jansen, J.A., and Mikos, A.G. Scaffold mesh size affects the osteoblastic differentiation of seeded marrow stromal cells cultured in a flow perfusion bioreactor. J Biomed Mater Res A **74,** 171, 2005.
20. Volkmer, E., Drosse, I., Otto, S., Stangelmayer, A., Stengele, M., Kallukalam, B., *et al.* Hypoxia in static and dynamic 3D culture systems for tissue engineering of bone. Tissue Eng Part A **14,** 1331, 2008.
21. Nam, Y.S., Yoon, J.J., and Park, T.G. A novel fabrication method of macroporous biodegradable polymer scaffolds using gas foaming salt as a porogen additive. J Biomed Mater Res **53,** 1, 2000.
22. Hou, Q., Grijpma, D.W., and Feijen, J. Preparation of interconnected highly porous polymeric structures by a replication and freeze-drying process. J Biomed Mater Res B Appl Biomater **67,** 732, 2003.
23. Yin, Y., Ye, F., Cui, J., Zhang, F., Li, X., and Yao, K. Preparation and characterization of macroporous chitosan-gelatin/beta-tricalcium phosphate composite scaffolds for bone tissue engineering. J Biomed Mater Res A **67,** 844, 2003.
24. Schugens, C., Maquet, V., Grandfils, C., Jerome, R., and Teyssie, P. Polylactide macroporous biodegradable implants for cell transplantation. II. Preparation of polylactide foams by liquid-liquid phase separation. J Biomed Mater Res **30,** 449, 1996.
25. Kim, H.J., Kim, U.J., Leisk, G.G., Bayan, C., Georgakoudi, I., and Kaplan, D.L. Bone regeneration on macroporous aqueous-derived silk 3-D scaffolds. Macromol Biosci **7,** 643, 2007.
26. Mikos, A.G., Thorsen, A.J., Czerwonka, L.A., Bao, Y., Langer, R., Winslow, D.N., *et al.* Preparation and characterization of poly(L-lactic acid) foams. Polymer **35,** 1068, 1994.
27. Shastri, V.P., Martin, I., and Langer, R. Macroporous polymer foams by hydrocarbon templating. Proc Natl Acad Sci U S A **97,** 1970, 2000.
28. Ma, P.X., and Choi, J.W. Biodegradable polymer scaffolds with well-defined interconnected spherical pore network. Tissue Eng **7,** 23, 2001.
29. Wei, G., and Ma, P.X. Macroporous and nanofibrous polymer scaffolds and polymer/bone-like apatite composite scaffolds generated by sugar spheres. J Biomed Mater Res A **78,** 306, 2006.
30. Martin, I., Shastri, V.P., Padera, R.F., Yang, J., Mackay, A.J., Langer, R., *et al.* Selective differentiation of mammalian bone marrow stromal cells cultured on three-dimensional polymer foams. J Biomed Mater Res **55,** 229, 2001.
31. Borden, M., Attawia, M., Khan, Y., and Laurencin, C. Tissue engineered microsphere-based matrices for bone repair: design and evaluation. Biomaterials **23,** 551–9. 2002.
32. Borden, M., Attawia, M., Khan, Y., El-Amin, S., and Laurencin, C. Tissue-engineered bone formation *in vivo* using a novel sintered polymeric microsphere matrix. J Bone Joint Surg Br **86,** 1200, 2004.
33. Jiang, T., Nukavarapu, S., Deng, M., Jabbarzadeh, E., Kofron, M., Doty, S., *et al.* Chitosan-poly(lactide-co-glycolide) microsphere-based scaffolds for bone tissue engineering: *in vitro* degradation and *in vivo* bone regeneration studies. Acta Biomater **6,** 3457, 2010.
34. Boschetti, F., Tomei, A.A., Turri, S., Swartz, M.A., and Levi, M. Design, fabrication, and characterization of a composite scaffold for bone tissue engineering. Int J Artif Organs **31,** 697, 2008.
35. Nukavarapu, S., Kumbar, S., Brown, J., Krogman, N., Weikel, A., Hindenlang, M., *et al.* Polyphosphazene/nano-hydroxyapatite composite microsphere scaffolds for bone tissue engineering. Biomacromolecules **9,** 1818, 2008.
36. Moore, M.J., Jabbari, E., Ritman, E.L., Lu, L., Currier, B.L., Windebank, A.J., *et al.* Quantitative analysis of interconnectivity of porous biodegradable scaffolds with micro-computed tomography. J Biomed Mater Res A **71,** 258, 2004.
37. ASTM Standard D1621. Standard Test Method for Compressive Properties of Rigid Cellular Plastics. West Conshohocken, PA: ASTM International, 2004.
38. Viktorov, I., and Proshin, S. Use of isopropyl alcohol in histological assays: dehydration of tissue, enbessing into paraffin, and processing of paraffin sections. Bull Exp Biol Med **136,** 105, 2003.
39. Athanasiou, K.A., Zhu, C., Lanctot, D.R., Agrawal, C.M., and Wang, X. Fundamentals of biomechanics in tissue engineering of bone. Tissue Eng **6,** 361, 2000.
40. Yu, H., Matthew, H.W., Wooley, P.H., and Yang, S.Y. Effect of porosity and pore size on microstructures and mechanical properties of poly-epsilon-caprolactone- hydroxyapatite composites. J Biomed Mater Res B Appl Biomater **86B,** 541, 2008.
41. Feng, B., Jinkang, Z., Zhen, W., Jianxi, L., Jiang, C., Jian, L., *et al.* The effect of pore size on tissue ingrowth and neovascularization in porous bioceramics of controlled architecture *in vivo*. Biomed Mater **6,** 015007, 2011.
42. Nukavarapu, S.P., Amini, A.R., and Wallace, J.S. Short-term and long-term effects of orthopedic biodegradable implants. J Long Term Eff Med Implants **21,** 93, 2011.
43. Murphy, C., and O'Brien, F. Understanding the effect of mean pore size on cell activity in collagen-glycosaminoglycan scaffolds. Cell Adh Migr **4,** 377, 2010.
44. Han, D., and Zhang, Q. An essential requirement for osteoclasts in refined bone-like tissue reconstruction *in vitro*. Med Hypotheses **67,** 75, 2006.
45. Druecke, D., Langer, S., Lamme, E., Pieper, J., Ugarkovic, M., Steinau, H.U., *et al.* Neovascularization of poly(ether ester) block-copolymer scaffolds *in vivo*: long-term investigations using intravital fluorescent microscopy. J Biomed Mater Res A **68,** 10, 2004.
46. Klenke, F.M., Liu, Y., Yuan, H., Hunziker, E.B., Siebenrock, K.A., and Hofstetter, W. Impact of pore size on the vascularization and osseointegration of ceramic bone substitutes *in vivo*. J Biomed Mater Res A **85,** 777, 2008.
47. Yaszemski, M.J., Payne, R.G., Hayes, W.C., Langer, R., and Mikos, A.G. Evolution of bone transplantation: molecular, cellular and tissue strategies to engineer human bone. Biomaterials **17,** 175, 1996.
48. Lv, Q., Nair, L., and Laurencin, C.T. Fabrication, characterization, and *in vitro* evaluation of poly(lactic acid glycolic acid)/nano-hydroxyapatite composite microsphere-based scaffolds for bone tissue engineering in rotating bioreactors. J Biomed Mater Res A **91,** 679, 2009.
49. Borden, M., Attawia, M., and Laurencin, C.T. The sintered microsphere matrix for bone tissue engineering: *in vitro* osteoconductivity studies. J Biomed Mater Res **61,** 421, 2002.

50. Borden, M., El-Amin, S.F., Attawia, M., and Laurencin, C.T. Structural and human cellular assessment of a novel microsphere-based tissue engineered scaffold for bone repair. Biomaterials **24,** 597, 2003.
51. Aydin, H.M., El Haj, A.J., Pişkin, E., and Yang, Y. Improving pore interconnectivity in polymeric scaffolds for tissue engineering. J Tissue Eng Regen Med **3,** 470, 2009.
52. Eiselt, P., Kim, B.S., Chacko, B., Isenberg, B., Peters, M.C., Greene, K.G., *et al.* Development of technologies aiding large-tissue engineering. Biotechnol Prog **14,** 134, 1998.
53. Granet, C., Laroche, N., Vico, L., Alexandre, C., and Lafage-Proust, M.H. Rotating-wall vessels, promising bioreactors for osteoblastic cell culture: comparison with other 3D conditions. Med Biol Eng Comput **36,** 513, 1998.
54. Yu, X., Botchwey, E.A., Levine, E.M., Pollack, S.R., and Laurencin, C.T. Bioreactor-based bone tissue engineering: the influence of dynamic flow on osteoblast phenotypic expression and matrix mineralization. Proc Natl Acad Sci U S A **101,** 11203, 2004.
55. Wang, E.A., Rosen, V., D'Alessandro, J.S., Bauduy, M., Cordes, P., Harada, T., *et al.* Recombinant human bone morphogenetic protein induces bone formation. Proc Natl Acad Sci U S A **87,** 2220, 1990.
56. Lucas, P.A., Laurencin, C., Syftestad, G.T., Domb, A., Goldberg, V.M., Caplan, A.I., *et al.* Ectopic induction of cartilage and bone by water-soluble proteins from bovine bone using a polyanhydride delivery vehicle. J Biomed Mater Res **24,** 901, 1990.
57. Laurencin, C.T., Attawia, M.A., Lu, L.Q., Borden, M.D., Lu, H.H., Gorum, W.J., *et al.* Poly(lactide-co-glycolide)/hydroxyapatite delivery of BMP-2-producing cells: a regional gene therapy approach to bone regeneration. Biomaterials **22,** 1271, 2001.
58. El-Ayoubi, R., Degrandpré, C., Diraddo, R., Yousefi, A.M., and Lavigne, P. Design and dynamic culture of 3D-scaffolds for cartilage tissue engineering. J Biomater Appl **25,** 429, 2011.

Address correspondence to:
Syam Nukavarapu, Ph.D.
Department of Orthopaedic Surgery
The University of Connecticut Health Center
263 Farmington Ave.
Farmington, CT 06030

E-mail: syam@uchc.edu

Received: February 7, 2011
Accepted: March 7, 2012
Online Publication Date: April 10, 2012